



An efficient, unconditionally energy stable local discontinuous Galerkin scheme for the Cahn–Hilliard–Brinkman system



Ruihan Guo¹, Yan Xu^{*,2}

School of Mathematical Sciences, University of Science and Technology of China, Hefei, Anhui 230026, PR China

ARTICLE INFO

Article history:

Received 19 January 2015
 Received in revised form 10 June 2015
 Accepted 12 June 2015
 Available online 18 June 2015

Keywords:

Cahn–Hilliard–Brinkman system
 Local discontinuous Galerkin method
 Energy stability
 Convex splitting
 Multigrid

ABSTRACT

In this paper, we present an efficient and unconditionally energy stable fully-discrete local discontinuous Galerkin (LDG) method for approximating the Cahn–Hilliard–Brinkman (CHB) system, which is comprised of a Cahn–Hilliard type equation and a generalized Brinkman equation modeling fluid flow. The semi-discrete energy stability of the LDG method is proved firstly. Due to the strict time step restriction ($\Delta t = \mathcal{O}(\Delta x^4)$) of explicit time discretization methods for stability, we introduce a semi-implicit scheme which consists of the implicit Euler method combined with a convex splitting of the discrete Cahn–Hilliard energy strategy for the temporal discretization. The unconditional energy stability of this fully-discrete convex splitting scheme is also proved. Obviously, the fully-discrete equations at the implicit time level are nonlinear, and to enhance the efficiency of the proposed approach, the nonlinear Full Approximation Scheme (FAS) multigrid method has been employed to solve this system of algebraic equations. We also show the nearly optimal complexity numerically. Numerical experiments based on the overall solution method of combining the proposed LDG method, convex splitting scheme and the nonlinear multigrid solver are given to validate the theoretical results and to show the effectiveness of the proposed approach for the CHB system.

© 2015 Elsevier Inc. All rights reserved.

1. Introduction

In this paper, we consider numerical methods in a bounded domain $\Omega \in \mathbb{R}^d$ ($d \leq 3$) for the Cahn–Hilliard–Brinkman (CHB) system:

$$\begin{aligned} \phi_t &= \nabla \cdot (M(\phi) \nabla \mu) - \nabla \cdot (\phi \mathbf{u}), \\ -\nabla \cdot [v(\phi) \mathbf{D}(\mathbf{u})] + \eta(\phi) \mathbf{u} &= -\nabla p - \gamma \phi \nabla \mu, \\ \nabla \cdot \mathbf{u} &= 0, \end{aligned} \quad (1.1)$$

where $M(\phi) > 0$ is a mobility that incorporates the Peclet number, $\gamma > 0$ is a surface tension parameter, \mathbf{u} is the advective velocity, p is the pressure, $v(\cdot) > 0$ is the fluid viscosity, $\eta(\cdot) > 0$ is the fluid permeability, $\mathbf{D}(\mathbf{u}) = \nabla \mathbf{u} + (\nabla \mathbf{u})^T$ and μ is the

* Corresponding author.

E-mail addresses: rguo@math.univ-lyon1.fr (R. Guo), yxu@ustc.edu.cn (Y. Xu).

¹ Current address: Institut Camille Jordan, Université Claude Bernard Lyon I, 43 boulevard 11 novembre 1918, 69622 Villeurbanne cedex, France.

² Research supported by NSFC grant No. 11371342.

chemical potential

$$\mu = \phi^3 - \phi - \varepsilon^2 \Delta \phi.$$

The CHB system is new enough, and there have been limited numerical simulations works in the existing literature. Collins et al. [12] presented an unconditionally energy stable and uniquely solvable finite difference scheme for the CHB system. Wise [28] introduced an unconditionally stable finite difference method for the Cahn–Hilliard–Hele–Shaw (CHHS) system. Guo et al. [18] developed an efficient fully-discrete local discontinuous Galerkin (LDG) method for the CHHS system. Feng and Wise [15] presented finite element analysis for a system of partial differential equations (PDEs) consisting of the Darcy equation and the Cahn–Hilliard (CH) equation. We know that when $\gamma = 0$, the CHB system is reduced to the CH equation [5], and many numerical methods have been developed to solve the CH equation, using finite elements [1–3], multigrid methods [19–21] and finite difference methods [14,16,26]. Xia et al. [29] developed an LDG method for the CH equation and proved the energy stability. Based on the LDG spatial discretization, Guo and Xu [17] studied the multigrid solver coupled with high order semi-implicit time marching method for the CH equation.

Solutions of the CHB system generally have boundary layers spread throughout the domain, so spatial resolution is extremely important in the choice of numerical schemes. The occurrence of the divergence free condition in the CHB system leads to the spatial resolution more difficult. In this paper, we introduce an LDG method to approximate the CHB system, which are high order accurate, nonlinear stable and flexible for arbitrary h and p adaptivity. The proof of the theoretical energy stability of the semi-discrete LDG scheme is also given in this paper.

The CHB system is difficult to approximate numerically due to the small time step size ($\Delta t = \mathcal{O}(\Delta x^4)$) required to maintain stability for explicit time integration methods. The major difficulty for the system is to find a suitable time integration method to improve the stability of the numerical simulation for large time steps. We develop a semi-implicit time integration scheme which consists of the implicit Euler method combined with a convex splitting of the discrete CH energy. The unconditional discrete energy stability of the fully-discrete convex splitting scheme has also been proved, i.e. the scheme is stable regardless of time step size. Being implicit in time, the equations at the implicit time level are nonlinear. The efficiency of the semi-implicit method highly depends on the efficiency of the nonlinear solver. In this paper, we demonstrate an efficient and practical nonlinear Full Approximation Scheme (FAS) multigrid method to solve the nonlinear equations arising by the semi-implicit scheme. In addition, we numerically show that the multigrid solver has optimal complexity for \mathcal{P}^1 approximation and nearly optimal complexity for \mathcal{P}^2 approximation.

The discontinuous Galerkin (DG) method we discuss in this paper is a class of finite element methods using completely discontinuous piecewise polynomial space for the numerical solution and the test functions in the spatial variables. Reed and Hill [25] first introduced the DG methods in 1973, in the framework of neutron linear transport. Later, it was developed for hyperbolic conservation laws containing first order derivatives by Cockburn et al. in a series of papers [6–9].

It is difficult to apply the DG method directly to PDEs containing higher order spatial derivatives, therefore the LDG method was introduced. The idea of the LDG method is to rewrite the equations with higher order derivatives as a first order system, then apply the DG method to the system. The first LDG method was constructed by Cockburn and Shu in [10] for solving a convection diffusion equation (containing second derivatives). Their work was motivated by the successful numerical experiments of Bassi and Rebay [4] for the compressible Navier–Stokes equations. Later, Yan and Shu developed an LDG method for a general KdV type equation (containing third order spatial derivatives) in [32], and they generalized the LDG method to PDEs with fourth and fifth order spatial derivatives in [33]. Xia et al. developed the LDG method to solve the Cahn–Hilliard type equations in [29] and extended the method in [30] to the more general application system which was coupled with the Allen–Cahn and Cahn–Hilliard equations. For a detailed description about the LDG methods for high-order time-dependent PDEs, we refer the readers to the review paper [31]. A common feature of these LDG methods is that stability can be proved for quite general nonlinear cases. DG and LDG methods also have several attractive properties, such as their flexibility for general geometry, unstructured meshes, arbitrary h and p adaptivity and their excellent parallel efficiency.

This paper is organized as follows. In Section 2, we develop an LDG method for the CHB system and prove the theoretical result of energy stability. In Section 3, we introduce a semi-implicit time integration method and prove the unconditional discrete energy stability for the fully-discrete scheme. In Section 4, we provide some results of numerical experiments validating our theoretical results and showing the effectiveness of the proposed LDG method, convex splitting scheme and the multigrid solver. Finally, we give concluding remarks in Section 5.

2. The LDG method for the Cahn–Hilliard–Brinkman system

2.1. Energy stability of the Cahn–Hilliard–Brinkman system

The CHB system was recently proposed to model phase separation and coarsening of a binary fluid in a Brinkman porous medium [24]. The CHB system on a bounded domain $\Omega \in \mathbb{R}^d$ ($d \leq 3$) is

$$\phi_t = \nabla \cdot (M(\phi) \nabla \mu) - \nabla \cdot (\phi \mathbf{u}), \quad (2.1a)$$

$$-\nabla \cdot [v(\phi) \mathbf{D}(\mathbf{u})] + \eta(\phi) \mathbf{u} = -\nabla p - \gamma \phi \nabla \mu, \quad (2.1b)$$

$$\nabla \cdot \mathbf{u} = 0, \quad (2.1c)$$

where μ is the chemical potential and given as

$$\mu := \delta_\phi E = \phi^3 - \phi - \varepsilon^2 \Delta \phi, \tag{2.2}$$

and the Ginzburg–Landau free energy E is given by

$$E(\phi) = \int_{\Omega} \left\{ \frac{\varepsilon^2}{2} |\nabla \phi|^2 + \frac{1}{4} (\phi^2 - 1)^2 \right\} d\mathbf{x}. \tag{2.3}$$

In the CHB system, ϕ denotes the concentration field and ε is a positive constant. The phase equilibria are presented by the pure fluids $\phi = \pm 1$. We assume that $M, \nu, \eta \in C^\infty$, and $M(\mathbf{x}) \geq M_0 > 0, \eta(\mathbf{x}) \geq \eta_0 > 0$ and $\nu(\mathbf{x}) \geq \nu_0 > 0$, for all \mathbf{x} . For example, we shall frequently use a regularized degenerate mobility of the form

$$M(\phi) = \frac{1}{\text{Pe}} \sqrt{(1 + \phi)^2 (1 - \phi)^2 + \varepsilon^2} \geq \frac{\varepsilon}{\text{Pe}} > 0, \tag{2.4}$$

where $\text{Pe} > 0$ is the Peclet number. To close the system, we assume that the system (2.1) is supplemented with the following Dirichlet boundary conditions for velocity \mathbf{u} , i.e.

$$\mathbf{u} = \mathbf{0} \quad \text{on} \quad \partial\Omega, \tag{2.5}$$

and Neumann boundary conditions for ϕ and μ , i.e.

$$\partial_n \phi = \partial_n \mu = 0 \quad \text{on} \quad \partial\Omega. \tag{2.6}$$

The Neumann boundary conditions (2.6) represent local thermodynamic equilibrium on the boundary. With the above boundary conditions, the CHB system (2.1) is mass conservative and energy dissipative, i.e.

$$\frac{d}{dt} E = - \int_{\Omega} \left(M(\phi) |\nabla \mu|^2 + \frac{1}{\gamma} \eta(\phi) |\mathbf{u}|^2 + \frac{1}{2\gamma} \nu(\phi) |D(\mathbf{u})|^2 \right) d\mathbf{x} \leq 0. \tag{2.7}$$

When the surface tension vanishes, i.e. $\gamma = 0$, the CHB system reduces to the Cahn–Hilliard equation [5], and when $\eta = 0$, equation (2.1b) is a Stokes type equation. The Cahn–Hilliard–Hele–Shaw system is obtained by setting $\nu = 0$ in equation (2.1b). The CHB system is a simplified version of the model derived by Lee et al. [22,23], which was used to describe gravity-driven, density-mismatched, two-phase flow in a Hele–Shaw cell.

2.2. The LDG method for the Cahn–Hilliard–Brinkman system

In this section, we consider the LDG method for the CHB system in $\Omega \in \mathbb{R}^d$ with $d \leq 3$. Although we do not perform numerical experiments in three dimensions in this paper, the LDG method and the energy stability results of this paper are all valid for $d \leq 3$.

2.2.1. Notations

Let \mathcal{T}_h denote a tessellation of Ω with shape-regular elements K . Let Γ denote the union of the boundary faces of elements $K \in \mathcal{T}_h$, i.e. $\Gamma = \cup_{K \in \mathcal{T}_h} \partial K$, and $\Gamma_0 = \Gamma \setminus \partial\Omega$. In order to describe the flux functions we need to introduce some notations. Let e be a face shared by the “left” and “right” elements K_L and K_R . For our purpose “left” and “right” can be uniquely defined for each face according to any fixed rule, see, e.g. [31,32] for more details of such a definition. Define the normal vectors \mathbf{v}_L and \mathbf{v}_R on e pointing exterior to K_L and K_R , respectively. If ψ is a function on K_L and K_R , but possibly discontinuous across e , let ψ_L denote $(\psi|_{K_L})|_e$ and ψ_R denote $(\psi|_{K_R})|_e$, the left and right trace, respectively.

Let $\mathcal{P}^k(K)$ be the space of polynomials of degree at most $k \geq 0$ on $K \in \mathcal{T}_h$. The finite element spaces are denoted by

$$\begin{aligned} V_h &= \left\{ \varphi : \varphi|_K \in \mathcal{P}^k(K), \quad \forall K \in \mathcal{T}_h \right\}, \\ \Sigma_h^d &= \left\{ \Phi = (\phi_1, \dots, \phi_d)^T : \phi_l|_K \in \mathcal{P}^k(K), \quad l = 1 \dots d, \quad \forall K \in \mathcal{T}_h \right\}, \\ \Pi_h^d &= \left\{ \Theta = (\theta_1, \dots, \theta_d)^T : \theta_l|_K \in (\mathcal{P}^k(K))^d, \quad l = 1 \dots d, \quad \forall K \in \mathcal{T}_h \right\}. \end{aligned}$$

Note that functions in V_h, Σ_h^d and Π_h^d are allowed to be completely discontinuous across element interfaces.

2.2.2. The LDG method

To construct the LDG method, firstly we rewrite the Cahn–Hilliard–Brinkman system (2.1) as a system containing only first order derivatives:

$$\phi_t = \nabla \cdot \mathbf{w}_1 - \nabla \cdot \mathbf{s}, \quad \mathbf{w}_1 = M(\phi) \mathbf{w}, \quad \mathbf{w} = \nabla \mu, \quad \mu = \phi^3 - \phi - \varepsilon^2 \nabla \cdot \mathbf{v}, \tag{2.8a}$$

$$\mathbf{v} = \nabla \phi, \quad \mathbf{s} = \phi \mathbf{u}, \quad \mathbf{0} = \nabla \cdot \mathbf{u}, \quad \mathbf{r} = \phi \mathbf{w}, \quad \mathbf{q} = \eta(\phi) \mathbf{u}, \tag{2.8b}$$

$$\mathbf{q} - \nabla \cdot \mathbf{Q} = -\nabla p - \gamma \mathbf{r}, \quad \mathbf{Q} = \nu(\phi) D(\mathbf{u}), \quad D(\mathbf{u}) = \nabla \mathbf{u} + (\nabla \mathbf{u})^T. \tag{2.8c}$$

Applying the LDG method to system (2.8), we have the scheme: Find $\phi, \mu, p \in V_h, \mathbf{w}_1, \mathbf{w}, \mathbf{v}, \mathbf{s}, \mathbf{q}, \mathbf{u}, \mathbf{r} \in \Sigma_h^d$ and $\mathbf{Q}, \mathbf{D}(\mathbf{u}) \in \Pi_h^d$, such that, for all test functions $\varphi_1, \varphi_2, \varphi_3 \in V_h, \boldsymbol{\eta}, \boldsymbol{\eta}_1, \boldsymbol{\eta}_2, \boldsymbol{\eta}_3, \boldsymbol{\eta}_4, \boldsymbol{\eta}_5, \boldsymbol{\eta}_6 \in \Sigma_h^d$ and $\boldsymbol{\Theta}_1, \boldsymbol{\Theta}_2 \in \Pi_h^d$, we have

$$\int_K \phi_t \varphi_1 dK = - \int_K (\mathbf{w}_1 - \mathbf{s}) \cdot \nabla \varphi_1 dK + \int_{\partial K} (\widehat{\mathbf{w}}_1 \cdot \mathbf{v} - \widehat{\mathbf{s}} \cdot \mathbf{v}) \varphi_1 ds, \tag{2.9a}$$

$$\int_K \mathbf{w}_1 \cdot \boldsymbol{\eta} dK = \int_K M(\phi) \mathbf{w} \cdot \boldsymbol{\eta} dK, \tag{2.9b}$$

$$\int_K \mathbf{w} \cdot \boldsymbol{\eta}_1 dK = - \int_K \mu \nabla \cdot \boldsymbol{\eta}_1 dK + \int_{\partial K} \widehat{\mu} \boldsymbol{\eta}_1 \cdot \mathbf{v} ds, \tag{2.9c}$$

$$\int_K \mu \varphi_2 dK = \int_K (\phi^3 - \phi) \varphi_2 dK + \int_K \varepsilon^2 \mathbf{v} \cdot \nabla \varphi_2 dK - \int_{\partial K} \varepsilon^2 \widehat{\mathbf{v}} \cdot \mathbf{v} \varphi_2 ds, \tag{2.9d}$$

$$\int_K \mathbf{v} \cdot \boldsymbol{\eta}_2 dK = - \int_K \phi \nabla \cdot \boldsymbol{\eta}_2 dK + \int_{\partial K} \widehat{\phi} \boldsymbol{\eta}_2 \cdot \mathbf{v} ds, \tag{2.9e}$$

$$\int_K \mathbf{s} \cdot \boldsymbol{\eta}_3 dK = \int_K \phi \mathbf{u} \cdot \boldsymbol{\eta}_3 dK, \tag{2.9f}$$

$$0 = - \int_K \mathbf{u} \cdot \nabla \varphi_3 dK + \int_{\partial K} \widehat{\mathbf{u}}_p \cdot \mathbf{v} \varphi_3 ds, \tag{2.9g}$$

$$\int_K \mathbf{r} \cdot \boldsymbol{\eta}_4 dK = \int_K \phi \mathbf{w} \cdot \boldsymbol{\eta}_4 dK, \tag{2.9h}$$

$$\int_K \mathbf{q} \cdot \boldsymbol{\eta}_5 dK = \int_K \eta(\phi) \mathbf{u} \cdot \boldsymbol{\eta}_5 dK, \tag{2.9i}$$

$$\int_K (\mathbf{q} + \gamma \mathbf{r}) \cdot \boldsymbol{\eta}_6 dK = \int_K (p \nabla \cdot \boldsymbol{\eta}_6 - \mathbf{Q} \cdot \nabla \boldsymbol{\eta}_6) dK + \int_{\partial K} (\widehat{\mathbf{Q}} \cdot \mathbf{v} \cdot \boldsymbol{\eta}_6 - \widehat{p} \boldsymbol{\eta}_6 \cdot \mathbf{v}) ds, \tag{2.9j}$$

$$\int_K \mathbf{Q} \cdot \boldsymbol{\Theta}_1 dK = \int_K v(\phi) \mathbf{D}(\mathbf{u}) \cdot \boldsymbol{\Theta}_1 dK, \tag{2.9k}$$

$$\int_K \mathbf{D}(\mathbf{u}) \cdot \boldsymbol{\Theta}_2 dK = - \int_K \mathbf{u} \cdot (\nabla \cdot \boldsymbol{\Theta}_2 + \nabla \cdot \boldsymbol{\Theta}_2^T) dK + \int_{\partial K} \widehat{\mathbf{u}} \cdot (\boldsymbol{\Theta}_2 \cdot \mathbf{v} + \boldsymbol{\Theta}_2^T \cdot \mathbf{v}) ds. \tag{2.9l}$$

The ‘‘hat’’ terms in (2.9) in the cell boundary terms from integration by parts are the so-called ‘‘numerical fluxes’’, which are functions defined on the edges and should be designed based on different guiding principles for different PDEs to ensure stability and local solvability of the intermediate variables. For CHB equation with periodic boundary conditions, similar to the development in [18], it turns out that we can take the simple choices such as

$$\begin{aligned} \widehat{\mathbf{w}}_1|_e &= \mathbf{w}_{1L}, \quad \widehat{\mathbf{s}}|_e = \mathbf{s}_L, \quad \widehat{\mu}|_e = \mu_R, \quad \widehat{\phi}|_e = \phi_L, \\ \widehat{\mathbf{v}}|_e &= \mathbf{v}_R, \quad \widehat{\mathbf{u}}|_e = \mathbf{u}_R, \quad \widehat{\mathbf{u}}_p|_e = \mathbf{u}_R, \quad \widehat{p}|_e = p_L, \quad \widehat{\mathbf{Q}}|_e = \mathbf{Q}_L. \end{aligned} \tag{2.10}$$

We remark that the choice for the fluxes (2.10) is not unique. Considering the compactness of the stencil and the optimal accuracy, the crucial part is taking $\widehat{\mathbf{w}}_1, \widehat{\mathbf{s}}$ and $\widehat{\mu}$ from opposite sides, $\widehat{\mathbf{v}}$ and $\widehat{\phi}$ from opposite sides, $\widehat{\mathbf{u}}_p$ and \widehat{p} from opposite sides, $\widehat{\mathbf{u}}$ and $\widehat{\mathbf{Q}}$ from opposite sides.

Remark 2.1. For CHB equation with boundary conditions (2.5)–(2.6), similar to the development of LDG method for Stokes system in [11], the numerical flux should be chosen as

$$\begin{aligned} \widehat{\mathbf{w}}_1|_e &= \mathbf{w}_{1L}, \quad \widehat{\mathbf{s}}|_e = \mathbf{s}_L, \quad \widehat{\mu}|_e = \mu_R, \quad \widehat{\phi}|_e = \phi_L, \quad \widehat{\mathbf{v}}|_e = \mathbf{v}_R, \\ \widehat{\mathbf{u}}|_e &= \mathbf{u}_R, \quad \widehat{\mathbf{Q}}|_e = \mathbf{Q}_L, \quad \widehat{\mathbf{u}}_p|_e = \mathbf{u}_R + D_{11}[p], \quad \widehat{p}|_e = p_L, \end{aligned} \tag{2.11}$$

where $[p] = p_R \mathbf{v}_R + p_L \mathbf{v}_L$ and the parameter D_{11} is chosen as $\mathcal{O}(\Delta x)$.

By the boundary (2.5)–(2.6), we take

$$\begin{aligned} \widehat{\mathbf{w}}_1 &= \mathbf{0}, \quad \widehat{\mathbf{s}} = \mathbf{0}, \quad \widehat{\mu} = \mu^{\text{in}}, \quad \widehat{\phi} = \phi^{\text{in}}, \quad \widehat{\mathbf{v}} = \mathbf{0}, \\ \widehat{\mathbf{u}} &= \mathbf{0}, \quad \widehat{\mathbf{Q}} = \mathbf{Q}^{\text{in}} - C_{11} \mathbf{u}^{\text{in}} \otimes \mathbf{v}^{\text{in}}, \quad \widehat{\mathbf{u}}_p = \mathbf{0}, \quad \widehat{p} = p^{\text{in}}, \end{aligned} \tag{2.12}$$

at the domain boundary, where ϕ^{in} means the value taken from the inside of the boundary element, \mathbf{v}^{in} is the unit normal vector pointing exterior to the boundary, and the parameter C_{11} is chosen as $\mathcal{O}(\frac{1}{\Delta x})$.

2.2.3. Energy dissipative

It is easy to show that the LDG scheme is mass conservative. And also we can prove the semi-discrete scheme is energy stable in the following.

Proposition 2.2 (Energy dissipative). *The solution to the LDG scheme (2.9) and the flux (2.10) satisfies the energy dissipative*

$$\frac{d}{dt} E = - \int_{\Omega} \left(M(\phi) |\mathbf{w}|^2 + \frac{1}{\gamma} \eta(\phi) |\mathbf{u}|^2 + \frac{1}{2\gamma} \nu(\phi) |D(\mathbf{u})|^2 \right) d\mathbf{x} \leq 0, \tag{2.13}$$

where

$$E = \int_{\Omega} \left(\frac{1}{4} (\phi^2 - 1)^2 + \frac{\varepsilon^2}{2} |\mathbf{v}|^2 \right) d\mathbf{x}. \tag{2.14}$$

Proof. Firstly, we take the time derivative of equation (2.9e) and choose the test function $\eta_2 = \varepsilon^2 \mathbf{v}$ to obtain

$$\varepsilon^2 \int_K \mathbf{v}_t \cdot \mathbf{v} dK = -\varepsilon^2 \int_K \phi_t \nabla \cdot \mathbf{v} dK + \varepsilon^2 \int_{\partial K} \widehat{\phi}_t \mathbf{v} \cdot \mathbf{v} ds. \tag{2.15}$$

For other equations in (2.9), we choose the test functions

$$\begin{aligned} \varphi_1 &= \mu, \quad \eta = -\mathbf{w}, \quad \eta_1 = \mathbf{w}_1 - \mathbf{s}, \quad \varphi_2 = -\phi_t, \quad \eta_3 = \mathbf{w}, \quad \varphi_3 = -\frac{1}{\gamma} p, \\ \eta_4 &= -\mathbf{u}, \quad \eta_5 = -\frac{1}{\gamma} \mathbf{u}, \quad \eta_6 = \frac{1}{\gamma} \mathbf{u}, \quad \Theta_1 = -\frac{1}{2\gamma} D(\mathbf{u}), \quad \Theta_2 = \frac{1}{2\gamma} \mathbf{Q}, \end{aligned}$$

respectively to get

$$\begin{aligned} \int_K \phi_t \mu dK &= - \int_K (\mathbf{w}_1 - \mathbf{s}) \cdot \nabla \mu dK + \int_{\partial K} (\widehat{\mathbf{w}}_1 \cdot \mathbf{v} - \widehat{\mathbf{s}} \cdot \mathbf{v}) \mu ds, \\ - \int_K \mathbf{w}_1 \cdot \mathbf{w} dK &= - \int_K M(\phi) \mathbf{w} \cdot \mathbf{w} dK, \\ \int_K \mathbf{w} \cdot (\mathbf{w}_1 - \mathbf{s}) dK &= - \int_K \mu \nabla \cdot (\mathbf{w}_1 - \mathbf{s}) dK + \int_{\partial K} \widehat{\mu} (\mathbf{w}_1 - \mathbf{s}) \cdot \mathbf{v} ds, \\ - \int_K \mu \phi_t dK &= - \int_K (\phi^3 - \phi) \phi_t dK - \int_K \varepsilon^2 \mathbf{v} \cdot \nabla \phi_t dK + \int_{\partial K} \varepsilon^2 \widehat{\mathbf{v}} \cdot \mathbf{v} \phi_t ds, \\ \int_K \mathbf{s} \cdot \mathbf{w} dK &= \int_K \phi \mathbf{u} \cdot \mathbf{w} dK, \\ 0 &= \frac{1}{\gamma} \int_K \mathbf{u} \cdot \nabla p dK - \frac{1}{\gamma} \int_{\partial K} \widehat{\mathbf{u}}_p \cdot \mathbf{v} p ds, \\ - \int_K \mathbf{r} \cdot \mathbf{u} dK &= - \int_K \phi \mathbf{w} \cdot \mathbf{u} dK, \\ - \frac{1}{\gamma} \int_K \mathbf{q} \cdot \mathbf{u} dK &= - \frac{1}{\gamma} \int_K \eta(\phi) \mathbf{u} \cdot \mathbf{u} dK, \end{aligned}$$

$$\begin{aligned} \frac{1}{\gamma} \int_K (\mathbf{q} + \gamma \mathbf{r}) \cdot \mathbf{u} dK &= \frac{1}{\gamma} \int_K (p \nabla \cdot \mathbf{u} - \mathbf{Q} \cdot \nabla \mathbf{u}) dK + \frac{1}{\gamma} \int_{\partial K} (\widehat{\mathbf{Q}} \cdot \mathbf{v} \cdot \mathbf{u} - \widehat{p} \mathbf{u} \cdot \mathbf{v}) ds, \\ -\frac{1}{2\gamma} \int_K \mathbf{Q} \cdot \mathbf{D}(\mathbf{u}) dK &= -\frac{1}{2\gamma} \int_K v(\phi) \mathbf{D}(\mathbf{u}) \cdot \mathbf{D}(\mathbf{u}) dK, \\ \frac{1}{2\gamma} \int_K \mathbf{D}(\mathbf{u}) \cdot \mathbf{Q} dK &= -\frac{1}{2\gamma} \int_K \mathbf{u} \cdot (\nabla \cdot \mathbf{Q} + \nabla \cdot \mathbf{Q}^T) dK + \frac{1}{2\gamma} \int_{\partial K} \widehat{\mathbf{u}} \cdot (\mathbf{Q} \cdot \mathbf{v} + \mathbf{Q}^T \cdot \mathbf{v}) ds. \end{aligned}$$

By the symmetric property of matrix \mathbf{Q} , we have

$$\frac{1}{2\gamma} \int_K \mathbf{D}(\mathbf{u}) \cdot \mathbf{Q} dK = -\frac{1}{\gamma} \int_K \mathbf{u} \cdot (\nabla \cdot \mathbf{Q}) dK + \frac{1}{\gamma} \int_{\partial K} \widehat{\mathbf{u}} \cdot (\mathbf{Q} \cdot \mathbf{v}) ds.$$

Combining the above equations with (2.15), implies

$$\begin{aligned} \frac{d}{dt} \int_K \left(\frac{1}{4}(\phi^2 - 1)^2 + \frac{\varepsilon^2}{2} |\mathbf{v}|^2 \right) dK &+ \int_K \left(M(\phi) |\mathbf{w}|^2 + \frac{1}{\gamma} \eta(\phi) |\mathbf{u}|^2 + \frac{1}{2\gamma} v(\phi) |\mathbf{D}(\mathbf{u})|^2 \right) dK \\ &= - \int_K \nabla \cdot (\mu(\mathbf{w}_1 - \mathbf{s})) dK + \int_{\partial K} ((\widehat{\mathbf{w}}_1 \cdot \mathbf{v} - \widehat{\mathbf{s}} \cdot \mathbf{v}) \mu + \widehat{\mu}(\mathbf{w}_1 - \mathbf{s}) \cdot \mathbf{v}) ds \\ &\quad - \int_K \varepsilon^2 \nabla \cdot (\phi_t \mathbf{v}) dK + \varepsilon^2 \int_{\partial K} (\widehat{\phi}_t \mathbf{v} \cdot \mathbf{v} + \widehat{\mathbf{v}} \cdot \mathbf{v} \phi_t) ds \\ &\quad + \frac{1}{\gamma} \int_K \nabla \cdot (p \mathbf{u}) dK - \frac{1}{\gamma} \int_{\partial K} (\widehat{\mathbf{u}}_p \cdot \mathbf{v} p + \widehat{p} \mathbf{u} \cdot \mathbf{v}) ds \\ &\quad - \frac{1}{\gamma} \int_K \nabla \cdot (\mathbf{Q} \cdot \mathbf{u}) dK + \frac{1}{\gamma} \int_{\partial K} (\widehat{\mathbf{Q}} \cdot \mathbf{v} \cdot \mathbf{u} + \widehat{\mathbf{u}} \cdot (\mathbf{Q} \cdot \mathbf{v})) ds. \end{aligned} \tag{2.16}$$

Finally, summing up equation (2.16) over K and noticing the fluxes in (2.10) are from the opposite sides of ∂K as well as the periodic boundary condition, we have

$$\frac{d}{dt} \int_{\Omega} \left(\frac{1}{4}(\phi^2 - 1)^2 + \frac{\varepsilon^2}{2} |\mathbf{v}|^2 \right) d\mathbf{x} + \int_{\Omega} \left(M(\phi) |\mathbf{w}|^2 + \frac{1}{\gamma} \eta(\phi) |\mathbf{u}|^2 + \frac{1}{2\gamma} v(\phi) |\mathbf{D}(\mathbf{u})|^2 \right) d\mathbf{x} = 0,$$

which implies the energy dissipative result (2.13). \square

3. Time discretization

In this section, we explore efficient semi-implicit time discretization techniques for the LDG scheme (2.9) to solve the CHB system. The main difficulty is the stiffness of the LDG spatial discretization operator, which would require an unreasonably small time step ($\Delta t = \mathcal{O}(\Delta x^4)$) for explicit local time stepping methods. It would therefore be desirable to develop semi-implicit time discretization techniques to relax this constraint of the time step.

3.1. Fully-discrete convex splitting scheme

In this subsection, we develop a semi-implicit scheme for the CHB system, which is based on a convex splitting approach of the discrete CH energy. The semi-discrete convex splitting scheme is given as

$$\frac{\phi^{n+1} - \phi^n}{\Delta t} = \nabla \cdot (M(\phi^n) \nabla \mu^{n+1}) - \nabla \cdot (\phi^n \mathbf{u}^{n+1}), \tag{3.1a}$$

$$\mu^{n+1} = (\phi^{n+1})^3 - \phi^n - \varepsilon^2 \Delta \phi^{n+1}, \tag{3.1b}$$

$$-\nabla \cdot [v(\phi^n) \mathbf{D}(\mathbf{u}^{n+1})] + \eta(\phi^n) \mathbf{u}^{n+1} = -\nabla p^{n+1} - \gamma \phi^n \nabla \mu^{n+1}, \tag{3.1c}$$

$$\nabla \cdot \mathbf{u}^{n+1} = 0. \tag{3.1d}$$

To define the LDG method for the scheme (3.1), we first rewrite it as a first order system

$$\frac{\phi^{n+1} - \phi^n}{\Delta t} = \nabla \cdot \mathbf{w}_1^{n+1} - \nabla \cdot \mathbf{s}^{n+1}, \quad \mathbf{w}_1^{n+1} = M(\phi^n) \mathbf{w}^{n+1}, \quad \mathbf{w}^{n+1} = \nabla \mu^{n+1}, \quad (3.2a)$$

$$\mathbf{s}^{n+1} = \phi^n \mathbf{u}^{n+1}, \quad \mu^{n+1} = (\phi^{n+1})^3 - \phi^n - \varepsilon^2 \nabla \cdot \mathbf{v}^{n+1}, \quad \mathbf{v}^{n+1} = \nabla \phi^{n+1}, \quad (3.2b)$$

$$\mathbf{r}^{n+1} = \phi^n \mathbf{w}^{n+1}, \quad \mathbf{q}^{n+1} = \eta(\phi^n) \mathbf{u}^{n+1}, \quad \mathbf{q}^{n+1} - \nabla \cdot \mathbf{Q}^{n+1} = -\nabla p^{n+1} - \gamma \mathbf{r}^{n+1}, \quad (3.2c)$$

$$\mathbf{Q}^{n+1} = \nu(\phi^n) \mathbf{D}(\mathbf{u}^{n+1}), \quad \mathbf{D}(\mathbf{u}^{n+1}) = \nabla \mathbf{u}^{n+1} + (\nabla \mathbf{u}^{n+1})^T, \quad 0 = \nabla \cdot \mathbf{u}^{n+1}. \quad (3.2d)$$

The LDG scheme for the semi-discrete scheme becomes: Find $\phi^{n+1}, \mu^{n+1}, p^{n+1} \in V_h, \mathbf{w}_1^{n+1}, \mathbf{w}^{n+1}, \mathbf{v}^{n+1}, \mathbf{s}^{n+1}, \mathbf{q}^{n+1}, \mathbf{u}^{n+1}, \mathbf{r}^{n+1} \in \Sigma_h^d$ and $\mathbf{Q}^{n+1}, \mathbf{D}(\mathbf{u}^{n+1}) \in \Pi_h^d$, such that, for all test functions $\varphi_1, \varphi_2, \varphi_3 \in V_h, \boldsymbol{\eta}, \boldsymbol{\eta}_1, \boldsymbol{\eta}_2, \boldsymbol{\eta}_3, \boldsymbol{\eta}_4, \boldsymbol{\eta}_5, \boldsymbol{\eta}_6 \in \Sigma_h^d$ and $\boldsymbol{\Theta}_1, \boldsymbol{\Theta}_2 \in \Pi_h^d$, we have

$$\int_K \frac{\phi^{n+1} - \phi^n}{\Delta t} \varphi_1 dK = - \int_K (\mathbf{w}_1^{n+1} - \mathbf{s}^{n+1}) \cdot \nabla \varphi_1 dK + \int_{\partial K} (\widehat{\mathbf{w}_1^{n+1}} \cdot \mathbf{v} - \widehat{\mathbf{s}^{n+1}} \cdot \mathbf{v}) \varphi_1 ds, \quad (3.3a)$$

$$\int_K \mathbf{w}_1^{n+1} \cdot \boldsymbol{\eta} dK = \int_K M(\phi^n) \mathbf{w}^{n+1} \cdot \boldsymbol{\eta} dK, \quad (3.3b)$$

$$\int_K \mathbf{w}^{n+1} \cdot \boldsymbol{\eta}_1 dK = - \int_K \mu^{n+1} \nabla \cdot \boldsymbol{\eta}_1 dK + \int_{\partial K} \widehat{\mu^{n+1}} \boldsymbol{\eta}_1 \cdot \mathbf{v} ds, \quad (3.3c)$$

$$\int_K \mu^{n+1} \varphi_2 dK = \int_K ((\phi^{n+1})^3 - \phi^n) \varphi_2 dK + \int_K \varepsilon^2 \mathbf{v}^{n+1} \cdot \nabla \varphi_2 dK - \int_{\partial K} \varepsilon^2 \widehat{\mathbf{v}^{n+1}} \cdot \mathbf{v} \varphi_2 ds, \quad (3.3d)$$

$$\int_K \mathbf{v}^{n+1} \cdot \boldsymbol{\eta}_2 dK = - \int_K \phi^{n+1} \nabla \cdot \boldsymbol{\eta}_2 dK + \int_{\partial K} \widehat{\phi^{n+1}} \boldsymbol{\eta}_2 \cdot \mathbf{v} ds, \quad (3.3e)$$

$$\int_K \mathbf{s}^{n+1} \cdot \boldsymbol{\eta}_3 dK = \int_K \phi^n \mathbf{u}^{n+1} \cdot \boldsymbol{\eta}_3 dK, \quad (3.3f)$$

$$0 = - \int_K \mathbf{u}^{n+1} \cdot \nabla \varphi_3 dK + \int_{\partial K} \widehat{\mathbf{u}_p^{n+1}} \cdot \mathbf{v} \varphi_3 ds, \quad (3.3g)$$

$$\int_K \mathbf{r}^{n+1} \cdot \boldsymbol{\eta}_4 dK = \int_K \phi^n \mathbf{w}^{n+1} \cdot \boldsymbol{\eta}_4 dK, \quad (3.3h)$$

$$\int_K \mathbf{q}^{n+1} \cdot \boldsymbol{\eta}_5 dK = \int_K \eta(\phi^n) \mathbf{u}^{n+1} \cdot \boldsymbol{\eta}_5 dK, \quad (3.3i)$$

$$\int_K (\mathbf{q}^{n+1} + \gamma \mathbf{r}^{n+1}) \cdot \boldsymbol{\eta}_6 dK = \int_K (p^{n+1} \nabla \cdot \boldsymbol{\eta}_6 - \mathbf{Q}^{n+1} \cdot \nabla \boldsymbol{\eta}_6) dK + \int_{\partial K} (\widehat{\mathbf{Q}^{n+1}} \cdot \mathbf{v} \cdot \boldsymbol{\eta}_6 - \widehat{p^{n+1}} \boldsymbol{\eta}_6 \cdot \mathbf{v}) ds, \quad (3.3j)$$

$$\int_K \mathbf{Q}^{n+1} \cdot \boldsymbol{\Theta}_1 dK = \int_K \nu(\phi^n) \mathbf{D}(\mathbf{u}^{n+1}) \cdot \boldsymbol{\Theta}_1 dK, \quad (3.3k)$$

$$\int_K \mathbf{D}(\mathbf{u}^{n+1}) \cdot \boldsymbol{\Theta}_2 dK = - \int_K \mathbf{u}^{n+1} \cdot (\nabla \cdot \boldsymbol{\Theta}_2 + \nabla \cdot \boldsymbol{\Theta}_2^T) dK + \int_{\partial K} \widehat{\mathbf{u}^{n+1}} \cdot (\boldsymbol{\Theta}_2 \cdot \mathbf{v} + \boldsymbol{\Theta}_2^T \cdot \mathbf{v}) ds. \quad (3.3l)$$

The numerical fluxes are

$$\begin{aligned} \widehat{\mathbf{w}_1^{n+1}}|_e &= \mathbf{w}_{1L}^{n+1}, & \widehat{\mathbf{s}^{n+1}}|_e &= \mathbf{s}_L^{n+1}, & \widehat{\mu^{n+1}}|_e &= \mu_R^{n+1}, & \widehat{\phi^{n+1}}|_e &= \phi_L^{n+1}, \\ \widehat{\mathbf{v}^{n+1}}|_e &= \mathbf{v}_R^{n+1}, & \widehat{\mathbf{u}^{n+1}}|_e &= \mathbf{u}_R^{n+1}, & \widehat{\mathbf{u}_p^{n+1}}|_e &= \mathbf{u}_R^{n+1}, & \widehat{p^{n+1}}|_e &= p_L^{n+1}, & \widehat{\mathbf{Q}^{n+1}}|_e &= \mathbf{Q}_L^{n+1}. \end{aligned} \quad (3.4)$$

The time discretization method which is based on a convex splitting of the discrete CH energy is similar what is described by Collins et al. in [12]. There is an important property that the convex splitting scheme generally inherit, unconditional energy stability. And the proof of the property will be given in Section 3.2.

3.2. Discrete energy dissipative

In this subsection, we will prove the unconditional discrete energy stability for the fully-discrete convex splitting scheme (3.3). To simplify the notation, we use the following notations for discretization of time variable,

$$\delta_t \phi^{n+1} = \frac{\phi^{n+1} - \phi^n}{\Delta t},$$

$$\delta_t \mathbf{v}^{n+1} = \frac{\mathbf{v}^{n+1} - \mathbf{v}^n}{\Delta t}.$$

Proposition 3.1 (Discrete energy dissipative). *The solution to the LDG scheme (3.3) and the flux (3.4) satisfies energy dissipative*

$$\int_{\Omega} \left(\frac{1}{4} ((\phi^{n+1})^2 - 1)^2 + \frac{\varepsilon^2}{2} |\mathbf{v}^{n+1}|^2 \right) d\mathbf{x} \leq \int_{\Omega} \left(\frac{1}{4} ((\phi^n)^2 - 1)^2 + \frac{\varepsilon^2}{2} |\mathbf{v}^n|^2 \right) d\mathbf{x}.$$

Proof. We take the test functions in (3.3) as

$$\varphi_1 = \mu^{n+1}, \quad \boldsymbol{\eta} = -\mathbf{w}^{n+1}, \quad \boldsymbol{\eta}_1 = \mathbf{w}_1^{n+1} - \mathbf{s}^{n+1}, \quad \varphi_2 = -\delta_t \phi^{n+1}, \quad \boldsymbol{\eta}_2 = \varepsilon^2 \delta_t \mathbf{v}^{n+1}, \quad \boldsymbol{\eta}_3 = \mathbf{w}^{n+1},$$

$$\varphi_3 = -\frac{1}{\gamma} p^{n+1}, \quad \boldsymbol{\eta}_4 = -\mathbf{u}^{n+1}, \quad \boldsymbol{\eta}_5 = -\frac{1}{\gamma} \mathbf{u}^{n+1}, \quad \boldsymbol{\eta}_6 = \frac{1}{\gamma} \mathbf{u}^{n+1}, \quad \boldsymbol{\Theta}_1 = -\frac{1}{2\gamma} \mathbf{D}(\mathbf{u}^{n+1}), \quad \boldsymbol{\Theta}_2 = \frac{1}{2\gamma} \mathbf{Q}^{n+1},$$

to obtain

$$\begin{aligned} \int_K \delta_t \phi^{n+1} \mu^{n+1} dK &= - \int_K (\mathbf{w}_1^{n+1} - \mathbf{s}^{n+1}) \cdot \nabla \mu^{n+1} dK + \int_{\partial K} (\widehat{\mathbf{w}_1^{n+1}} \cdot \mathbf{v} - \widehat{\mathbf{s}^{n+1}} \cdot \mathbf{v}) \mu^{n+1} ds, \\ - \int_K \mathbf{w}_1^{n+1} \cdot \mathbf{w}^{n+1} dK &= - \int_K M(\phi^n) \mathbf{w}^{n+1} \cdot \mathbf{w}^{n+1} dK, \\ \int_K \mathbf{w}^{n+1} \cdot (\mathbf{w}_1^{n+1} - \mathbf{s}^{n+1}) dK &= - \int_K \mu^{n+1} \nabla \cdot (\mathbf{w}_1^{n+1} - \mathbf{s}^{n+1}) dK + \int_{\partial K} \widehat{\mu}^{n+1} (\mathbf{w}_1^{n+1} - \mathbf{s}^{n+1}) \cdot \mathbf{v} ds, \\ - \int_K \mu^{n+1} \delta_t \phi^{n+1} dK &= - \int_K ((\phi^{n+1})^3 - \phi^n) \delta_t \phi^{n+1} dK \\ &\quad - \int_K \varepsilon^2 \mathbf{v}^{n+1} \cdot \nabla \delta_t \phi^{n+1} dK + \int_{\partial K} \varepsilon^2 \widehat{\mathbf{v}^{n+1}} \cdot \mathbf{v} \delta_t \phi^{n+1} ds, \\ \varepsilon^2 \int_K \mathbf{v}^{n+1} \cdot \delta_t \mathbf{v}^{n+1} dK &= -\varepsilon^2 \int_K \phi^{n+1} \nabla \cdot \delta_t \mathbf{v}^{n+1} dK + \varepsilon^2 \int_{\partial K} \widehat{\phi}^{n+1} \delta_t \mathbf{v}^{n+1} \cdot \mathbf{v} ds, \\ \int_K \mathbf{s}^{n+1} \cdot \mathbf{w}^{n+1} dK &= \int_K \phi^n \mathbf{u}^{n+1} \cdot \mathbf{w}^{n+1} dK, \\ 0 &= \frac{1}{\gamma} \int_K \mathbf{u}^{n+1} \cdot \nabla p^{n+1} dK - \frac{1}{\gamma} \int_{\partial K} \widehat{\mathbf{u}^{n+1}} \cdot \mathbf{v} p^{n+1} ds, \\ - \int_K \mathbf{r}^{n+1} \cdot \mathbf{u}^{n+1} dK &= - \int_K \phi^n \mathbf{w}^{n+1} \cdot \mathbf{u}^{n+1} dK, \\ - \frac{1}{\gamma} \int_K \mathbf{q}^{n+1} \cdot \mathbf{u}^{n+1} dK &= - \frac{1}{\gamma} \int_K \eta(\phi^n) \mathbf{u}^{n+1} \cdot \mathbf{u}^{n+1} dK, \\ \frac{1}{\gamma} \int_K (\mathbf{q}^{n+1} + \gamma \mathbf{r}^{n+1}) \cdot \mathbf{u}^{n+1} dK &= \frac{1}{\gamma} \int_K (p^{n+1} \nabla \cdot \mathbf{u}^{n+1} - \mathbf{Q}^{n+1} \cdot \nabla \mathbf{u}^{n+1}) dK \\ &\quad + \frac{1}{\gamma} \int_{\partial K} (\widehat{\mathbf{Q}^{n+1}} \cdot \mathbf{v} \cdot \mathbf{u}^{n+1} - \widehat{p}^{n+1} \mathbf{u}^{n+1} \cdot \mathbf{v}) ds, \end{aligned}$$

$$\begin{aligned}
 -\frac{1}{2\gamma} \int_K \mathbf{Q}^{n+1} \cdot \mathbf{D}(\mathbf{u}^{n+1}) dK &= -\frac{1}{2\gamma} \int_K v(\phi^n) \mathbf{D}(\mathbf{u}^{n+1}) \cdot \mathbf{D}(\mathbf{u}^{n+1}) dK, \\
 \frac{1}{2\gamma} \int_K \mathbf{D}(\mathbf{u}^{n+1}) \cdot \mathbf{Q}^{n+1} dK &= -\frac{1}{\gamma} \int_K \mathbf{u}^{n+1} \cdot (\nabla \cdot \mathbf{Q}^{n+1}) dK + \frac{1}{\gamma} \int_{\partial K} \widehat{\mathbf{u}}^{n+1} \cdot (\mathbf{Q}^{n+1} \cdot \mathbf{v}) ds.
 \end{aligned}$$

Combining the above equations, we get

$$\begin{aligned}
 \varepsilon^2 \int_K \mathbf{v}^{n+1} \cdot \delta_t \mathbf{v}^{n+1} dK &+ \int_K ((\phi^{n+1})^3 - \phi^n) \delta_t \phi^{n+1} dK \\
 &+ \int_K \left(M(\phi^n) |\mathbf{w}^{n+1}|^2 + \frac{1}{\gamma} \eta(\phi^n) |\mathbf{u}^{n+1}| + \frac{1}{2\gamma} v(\phi^n) |\mathbf{D}(\mathbf{u}^{n+1})|^2 \right) dK \\
 &= - \int_K \nabla \cdot (\mu^{n+1} (\mathbf{w}_1^{n+1} - \mathbf{s}^{n+1})) dK + \int_{\partial K} ((\widehat{\mathbf{w}}_1^{n+1} \cdot \mathbf{v} - \widehat{\mathbf{s}}^{n+1} \cdot \mathbf{v}) \mu^{n+1} \\
 &+ \widehat{\mu}^{n+1} (\mathbf{w}_1^{n+1} - \mathbf{s}^{n+1}) \cdot \mathbf{v}) ds + \frac{1}{\gamma} \int_K \nabla \cdot (p^{n+1} \mathbf{u}^{n+1}) dK - \frac{1}{\gamma} \int_{\partial K} (\widehat{\mathbf{u}}_p^{n+1} \cdot \mathbf{v} p^{n+1} \\
 &+ \widehat{p}^{n+1} \mathbf{u}^{n+1} \cdot \mathbf{v}) ds - \frac{1}{\gamma} \int_K \nabla \cdot (\mathbf{Q}^{n+1} \cdot \mathbf{u}^{n+1}) dK + \frac{1}{\gamma} \int_{\partial K} (\widehat{\mathbf{Q}}^{n+1} \cdot \mathbf{v} \cdot \mathbf{u}^{n+1} + \widehat{\mathbf{u}}^{n+1} \cdot (\mathbf{Q}^{n+1} \cdot \mathbf{v})) ds \\
 &- \frac{\varepsilon^2}{\Delta t} \int_K \nabla \cdot (\phi^{n+1} \mathbf{v}^{n+1}) dK + \frac{\varepsilon^2}{\Delta t} \int_{\partial K} (\widehat{\mathbf{v}}^{n+1} \cdot \mathbf{v} \phi^{n+1} + \widehat{\phi}^{n+1} \mathbf{v}^{n+1} \cdot \mathbf{v}) ds \\
 &+ \frac{\varepsilon^2}{\Delta t} \int_K (\mathbf{v}^{n+1} \cdot \nabla \phi^n + \phi^{n+1} \nabla \cdot \mathbf{v}^n) dK - \frac{\varepsilon^2}{\Delta t} \int_{\partial K} (\widehat{\mathbf{v}}^{n+1} \cdot \mathbf{v} \phi^n + \widehat{\phi}^{n+1} \mathbf{v}^n \cdot \mathbf{v}) ds.
 \end{aligned} \tag{3.5}$$

For equation (3.3e), we choose the test function as $\eta_2 = \mathbf{v}^n$, and obtain

$$\int_K \mathbf{v}^{n+1} \cdot \mathbf{v}^n dK = - \int_K \phi^{n+1} \nabla \cdot \mathbf{v}^n dK + \int_{\partial K} \widehat{\phi}^{n+1} \mathbf{v}^n \cdot \mathbf{v} ds. \tag{3.6}$$

From (3.3e), we have

$$\int_K \mathbf{v}^n \cdot \eta_2 dK = - \int_K \phi^n \nabla \cdot \eta_2 dK + \int_{\partial K} \widehat{\phi}^n \eta_2 \cdot \mathbf{v} ds. \tag{3.7}$$

Choosing the test function $\eta_2 = \mathbf{v}^{n+1}$ in (3.7), implies

$$\int_K \mathbf{v}^n \cdot \mathbf{v}^{n+1} dK = - \int_K \phi^n \nabla \cdot \mathbf{v}^{n+1} dK + \int_{\partial K} \widehat{\phi}^n \mathbf{v}^{n+1} \cdot \mathbf{v} ds. \tag{3.8}$$

By substituting (3.6) and (3.8), we have

$$\begin{aligned}
 &\int_K (\mathbf{v}^{n+1} \cdot \nabla \phi^n + \phi^{n+1} \nabla \cdot \mathbf{v}^n) dK - \int_{\partial K} (\widehat{\mathbf{v}}^{n+1} \cdot \mathbf{v} \phi^n + \widehat{\phi}^{n+1} \mathbf{v}^n \cdot \mathbf{v}) ds \\
 &\stackrel{(3.6)}{=} \int_K (\mathbf{v}^{n+1} \cdot \nabla \phi^n - \mathbf{v}^{n+1} \cdot \mathbf{v}^n) dK - \int_{\partial K} \widehat{\mathbf{v}}^{n+1} \cdot \mathbf{v} \phi^n ds \\
 &= \int_K (\mathbf{v}^{n+1} \cdot \nabla \phi^n - \mathbf{v}^{n+1} \cdot \mathbf{v}^n - \phi^n \nabla \cdot \mathbf{v}^{n+1} + \phi^n \nabla \cdot \mathbf{v}^{n+1}) dK - \int_{\partial K} \widehat{\mathbf{v}}^{n+1} \cdot \mathbf{v} \phi^n ds \\
 &\stackrel{(3.8)}{=} \int_K (\mathbf{v}^{n+1} \cdot \nabla \phi^n + \phi^n \nabla \cdot \mathbf{v}^{n+1}) dK - \int_{\partial K} (\widehat{\mathbf{v}}^{n+1} \cdot \mathbf{v} \phi^n + \widehat{\phi}^n \mathbf{v}^{n+1} \cdot \mathbf{v}) ds.
 \end{aligned} \tag{3.9}$$

Finally, summing up equations (3.5) and (3.9) over K and noticing the fluxes in (3.4) are from the opposite sides of ∂K as well as the boundary conditions, we get

$$\begin{aligned} &\varepsilon^2 \int_{\Omega} \mathbf{v}^{n+1} \cdot \delta_t \mathbf{v}^{n+1} \, d\mathbf{x} + \int_{\Omega} ((\phi^{n+1})^3 - \phi^n) \delta_t \phi^{n+1} \, d\mathbf{x} \\ &+ \int_{\Omega} \left(M(\phi^n) |\mathbf{w}^{n+1}|^2 + \frac{1}{\gamma} \eta(\phi^n) |\mathbf{u}|^{n+1} + \frac{1}{2\gamma} \nu(\phi^n) |D(\mathbf{u}^{n+1})|^2 \right) d\mathbf{x} = 0. \end{aligned}$$

Then

$$\begin{aligned} &\varepsilon^2 \int_{\Omega} \mathbf{v}^{n+1} \cdot \delta_t \mathbf{v}^{n+1} \, d\mathbf{x} + \frac{1}{\Delta t} \int_{\Omega} \left(\frac{1}{4} ((\phi^{n+1})^2 - 1)^2 \right) d\mathbf{x} - \frac{1}{\Delta t} \int_{\Omega} \left(\frac{1}{4} ((\phi^n)^2 - 1)^2 \right) d\mathbf{x} \\ &+ \frac{1}{4\Delta t} \int_{\Omega} \left((2 + 2(\phi^{n+1})^2 + (\phi^n + \phi^{n+1})^2) (-\phi^{n+1} + \phi^n)^2 \right) d\mathbf{x} \\ &+ \int_{\Omega} \left(M(\phi^n) |\mathbf{w}^{n+1}|^2 + \frac{1}{\gamma} \eta(\phi^n) |\mathbf{u}|^{n+1} + \frac{1}{2\gamma} \nu(\phi^n) |D(\mathbf{u}^{n+1})|^2 \right) d\mathbf{x} = 0, \end{aligned}$$

therefore we obtain the discrete energy stability

$$\int_{\Omega} \left(\frac{1}{4} ((\phi^{n+1})^2 - 1)^2 + \frac{\varepsilon^2}{2} |\mathbf{v}^{n+1}|^2 \right) d\mathbf{x} \leq \int_{\Omega} \left(\frac{1}{4} ((\phi^n)^2 - 1)^2 + \frac{\varepsilon^2}{2} |\mathbf{v}^n|^2 \right) d\mathbf{x}. \quad \square$$

Remark 3.2. The unconditional energy stability for the fully discrete convex splitting scheme (3.3) is proved, i.e. the scheme is stable regardless of time step size. But as for the solvability of the convex splitting scheme, the proof is not easy in the LDG framework. Even though the auxiliary variables in the LDG method give the easy treatment for nonlinear and high order derivative terms, the theoretical analysis of solvability for the LDG method is more troublesome because of the auxiliary variables. We will leave it to our future work.

Remark 3.3. Diegel et al. [13] studied the convergence analysis for the Cahn–Hilliard–Darcy–Stokes system, combined with a mixed finite element method in space. However, the convergence analysis for the convex splitting scheme in the LDG framework is difficult because of the auxiliary variables, which will be left to our future work.

Remark 3.4. The energy stability for the semi-discrete LDG scheme (2.9) and fully discrete convex splitting scheme (3.3) for variables ϕ and \mathbf{v} are proved in Proposition 2.2 and 3.1, respectively. The numerical solutions with LDG spatial discretization are discontinuous piecewise polynomial, which leads to that the numerical solutions for ϕ and \mathbf{v} are in $L^2(\Omega)$ space, but not in $H^1(\Omega)$ space. Therefore, H^1 -stability for the numerical solution ϕ will not be proved.

3.3. Algorithm flowchart and the multigrid solver

Given ϕ^n, μ^n, p^n and \mathbf{u}^n , the algorithm to get $\phi^{n+1}, \mu^{n+1}, p^{n+1}$ and \mathbf{u}^{n+1} is as follows

1. We choose a local basis in cell K , then $\mathbf{w}_1^{n+1}, \mathbf{w}^{n+1}, \mathbf{v}^{n+1}, \mathbf{s}^{n+1}, \mathbf{r}^{n+1}, \mathbf{q}^{n+1}, \mathbf{Q}^{n+1}$ and $D(\mathbf{u}^{n+1})$ can be eliminated from equations (3.3b), (3.3c), (3.3e), (3.3f), (3.3h), (3.3i), (3.3k) and (3.3l) respectively, by simply inverting a small mass matrix in each case.
2. We get a system of $3 + d$ (d is the dimension of the problem) coupled nonlinear equations for $\{\phi^{n+1}, \mu^{n+1}, p^{n+1}, \mathbf{u}^{n+1}\}$

$$\begin{cases} \phi^{n+1} = L_1(\mu^{n+1}, \mathbf{u}^{n+1}, \phi^n), \\ \mu^{n+1} = L_2(\phi^{n+1}, \phi^n), \\ L_3(\mathbf{u}^{n+1}) = 0, \\ L_4(\mu^{n+1}, \mathbf{u}^{n+1}, p^{n+1}, \phi^n) = 0. \end{cases} \tag{3.10}$$

3. We solve the system of nonlinear equations (3.10) at each time step and get $\phi^{n+1}, \mu^{n+1}, p^{n+1}$ and \mathbf{u}^{n+1} .

The semi-implicit convex splitting scheme (3.1) is stable regardless of time step size. However, the scheme is nonlinear, and we need to solve a system of nonlinear algebraic equations (3.10) at each time step, which presents a challenge regarding practical implementation. The overall performance highly depends on the performance of the solver. Traditional iterative solution methods such as Gauss–Seidel method and Newton method suffer from slow convergence rates, especially for large algebraic systems.

The nonlinear FAS multigrid method is employed here to solve the nonlinear equations and we will numerically show the nearly optimal convergence of the multigrid solver in the next section. The reader is referred to Trottenberg et al. [27] for complete details of the nonlinear FAS multigrid algorithm.

Table 4.1

Accuracy test for Example 4.1 at $t = 0.5$. To maintain the accuracy, the time step is chosen as $\Delta t = 0.1\Delta x$, $\Delta t = 0.4\Delta x^2$ and $\Delta t = 0.4\Delta x^3$ for \mathcal{P}^0 , \mathcal{P}^1 and \mathcal{P}^2 approximation, respectively.

	N	$\varepsilon = 1.0, \gamma = 1.0$				$\varepsilon = 0.2, \gamma = 2.0$			
		L^2 error	order	L^∞ error	order	L^2 error	order	L^∞ error	order
\mathcal{P}^0	8	4.90E-01	–	1.90E-01	–	9.06E-01	–	2.83E-01	–
	16	2.31E-01	1.08	9.16E-02	1.05	3.52E-01	1.36	1.66E-01	0.77
	32	1.11E-01	1.05	4.41E-02	1.05	1.47E-01	1.25	7.23E-02	1.19
	64	5.47E-02	1.02	2.18E-02	1.01	6.63E-02	1.15	3.36E-02	1.10
\mathcal{P}^1	8	5.21E-01	–	2.26E-01	–	5.36E-01	–	1.87E-01	–
	16	1.55E-01	1.74	6.42E-02	1.82	1.62E-01	1.72	4.70E-02	1.99
	32	4.15E-02	1.90	1.68E-02	1.94	4.88E-02	1.73	1.45E-02	1.69
	64	1.06E-02	1.97	4.27E-03	1.98	1.32E-02	1.88	4.10E-03	1.83
\mathcal{P}^2	8	3.80E-01	–	1.24E-01	–	3.84E-01	–	1.06E-01	–
	16	6.34E-02	2.59	2.02E-02	2.62	7.16E-02	2.43	1.96E-02	2.44
	32	8.30E-03	2.93	2.62E-03	2.95	1.04E-02	2.78	3.10E-03	2.66
	64	1.04E-03	2.99	3.29E-04	2.99	1.33E-03	2.97	4.02E-04	2.95

4. Numerical tests

In this section, we perform numerical experiments of the LDG method applied to the Cahn–Hilliard–Brinkman system. We consider the convex splitting scheme (3.3) and the resulting nonlinear equations are solved by the FAS multigrid method. For the spatial discretization, we use uniform meshes. All the computations are performed in double precision.

Example 4.1 (Convergence of the multigrid solver). To demonstrate the convergence and nearly optimal complexity of the multigrid solver, we provide evidence that the multigrid convergence rate is nearly independent of the grid size Δx . For the tests we take the exact solution of

$$\phi(x, y, t) = e^{-2t} \sin(x) \sin(y), \tag{4.1}$$

with the source term $f(x, y, t)$, where $f(x, y, t)$ is a given function so that make the exact solution. The initial condition is

$$\phi(x, y, 0) = \sin(x) \sin(y), \tag{4.2}$$

and the domain is $[0, 2\pi] \times [0, 2\pi]$ with periodic boundary conditions. The spatial step size varies from $\Delta x = 2\pi/32$ to $\Delta x = 2\pi/128$ in the test results.

The only one tunable parameter in our multigrid solver is λ , i.e. the number of multigrid smoothing sweeps. We present the convergence rates of the multigrid solver at the 10th time step for various choices of λ in Fig. 4.1. Three different values for λ , namely, 3, 4 and 5 are used. We choose $M = 1$, $\varepsilon = 0.1$ and $\gamma = 2.0$ in our tests.

From Fig. 4.1, we can see the optimal convergence of the multigrid solver for \mathcal{P}^1 approximation and nearly optimal convergence for \mathcal{P}^2 approximation, with $\lambda = 4$ and $\lambda = 5$. While for $\lambda = 3$ and \mathcal{P}^2 approximation, we do not observe a similar feature. Significantly more multigrid iterations are required for smaller values of spatial step size Δx .

The L^2 and L^∞ errors and numerical orders of accuracy at time $t = 0.5$ are contained in Table 4.1. To maintain the accuracy, the time step is chosen as $\Delta t = 0.1\Delta x$, $\Delta t = 0.4\Delta x^2$ and $\Delta t = 0.4\Delta x^3$ for \mathcal{P}^0 , \mathcal{P}^1 and \mathcal{P}^2 approximation, respectively. We can see that the method with \mathcal{P}^k elements gives $(k + 1)$ th order of accuracy in both L^2 and L^∞ norms. What we should keep in mind is that the choice of this refinement path has nothing to do with any time step restriction for stability.

Example 4.2 (Spinodal decomposition). Here we present a couple of simulations of spinodal decomposition. The energy dissipation is demonstrated at the numerical level and we show the effect of different values of the parameter γ . We consider the convex splitting scheme (3.1) with the LDG spatial discretization with \mathcal{P}^2 approximation on a 128×128 mesh and boundary conditions (2.5)–(2.6). The initial data is a random field of values that are uniformly distributed about the average composition $\bar{\phi} = -0.05$, with amplitude 0.05. The domain is $[0, 6.4] \times [0, 6.4]$. We take

$$M(\phi) = \sqrt{(1 + \phi)^2(1 - \phi)^2 + \epsilon^2}, \quad \epsilon = 0.03, \quad \eta = 1 \quad \text{and} \quad \nu = 1.$$

For γ we use the values 0.0 and 4.0.

Fig. 4.2 shows the simulations with different γ at times $t = 1.0, 4.0, 12.0$ and 20.0 . From Fig. 4.2, we can see that identified particles have a smaller shaper factor for $\gamma = 4.0$ than for $\gamma = 0.0$ when compared at the same time. In spinodal decomposition, particles can coarsen, i.e. large particles may grow at the expense of smaller particles. Fig. 4.2 shows statistically similar patterns in the numerical solution as those in Collins et al. [12].

The computed discrete energy trace with different γ is presented in Fig. 4.3. We can see that the discrete energy is non-increasing in time, which agrees with the theoretical result. In addition, in the early stages of decomposition, the energy is closely matched. Then in the latter stages of decomposition, the energy decrease faster for larger γ . What we

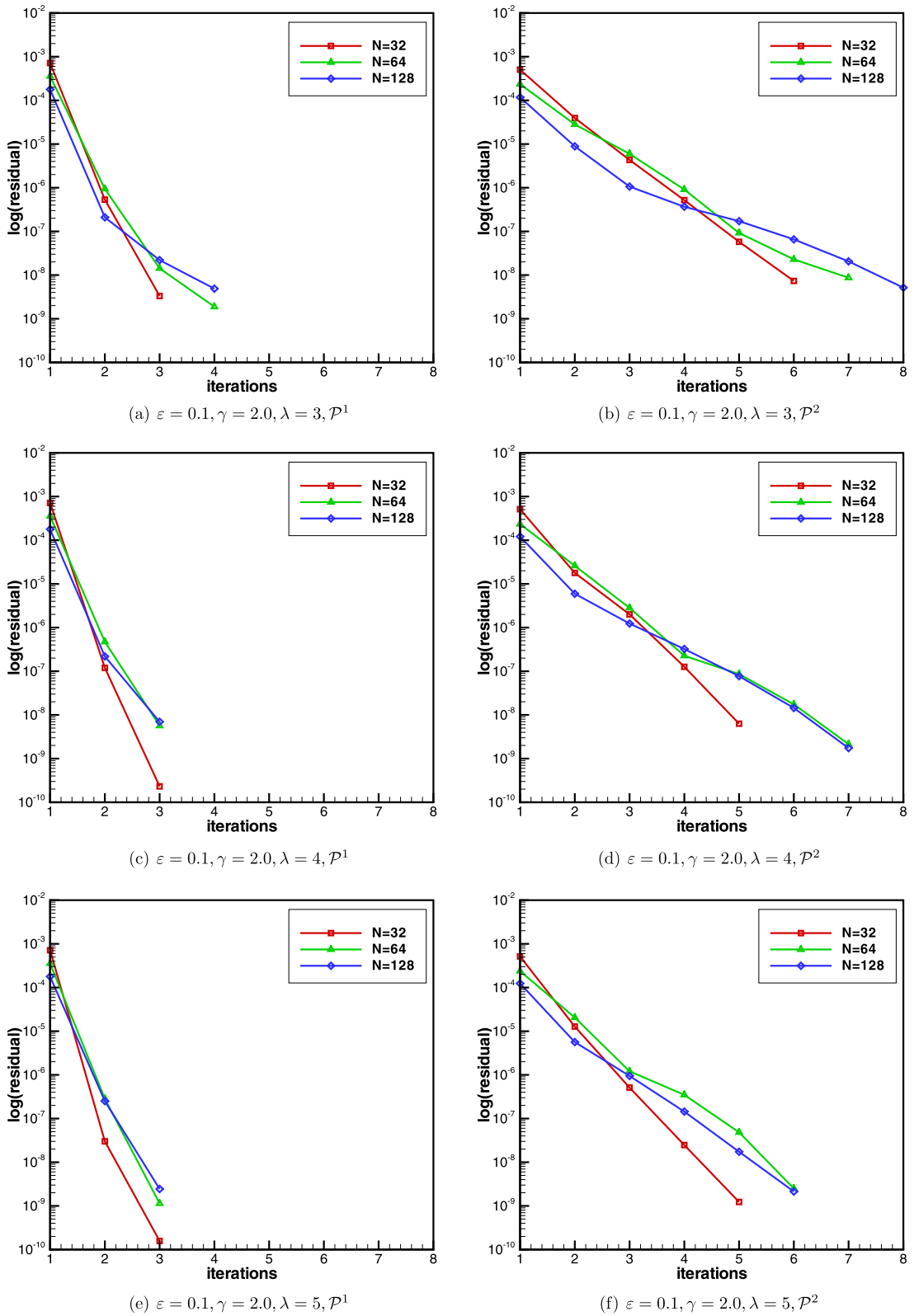


Fig. 4.1. Convergence rates of multigrid solver with \mathcal{P}^1 and \mathcal{P}^2 approximation for various choices of λ .

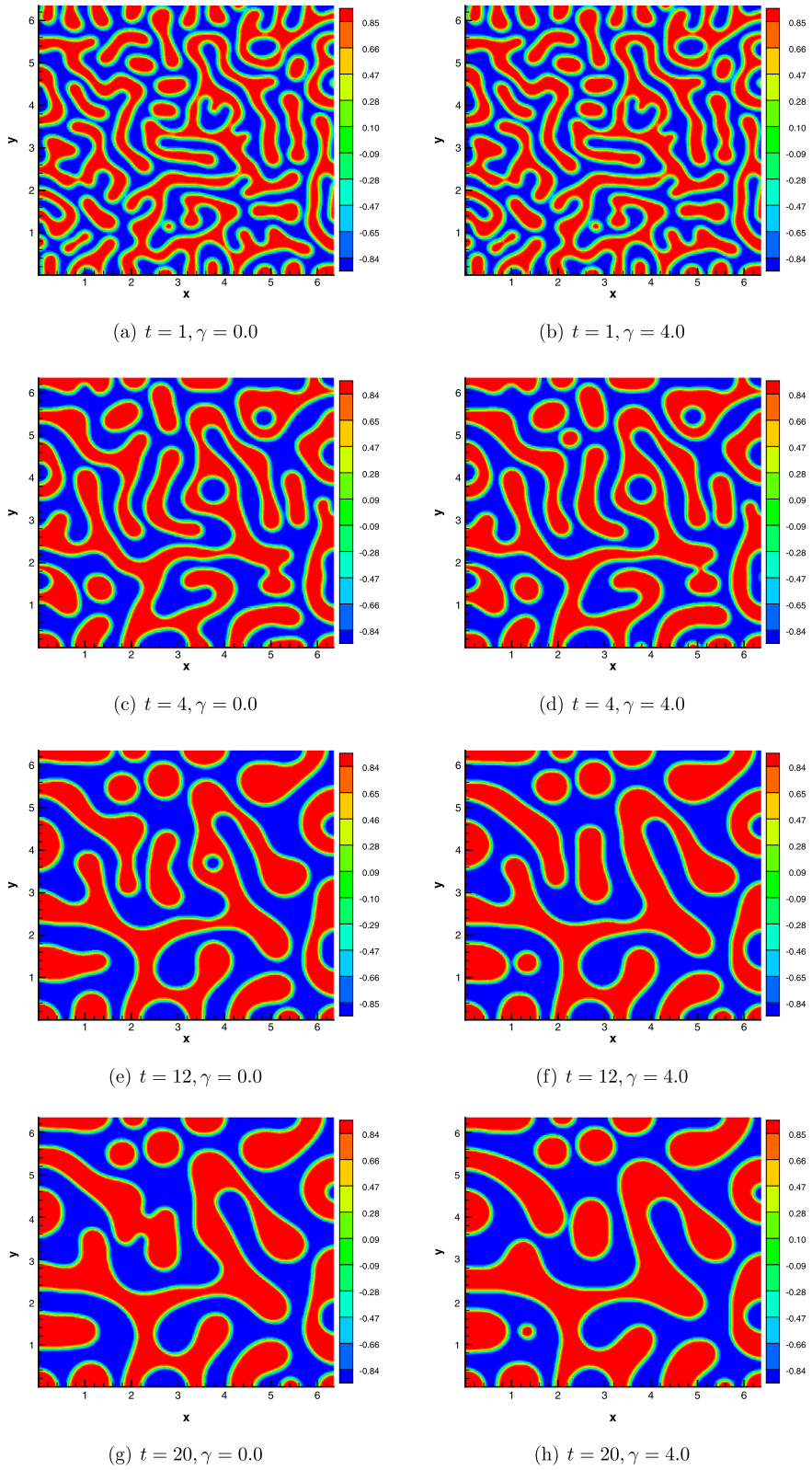


Fig. 4.2. The time evolution of the CHB system implemented with scheme (3.1) with \mathcal{P}^2 approximation on a 128×128 mesh for Example 4.2.

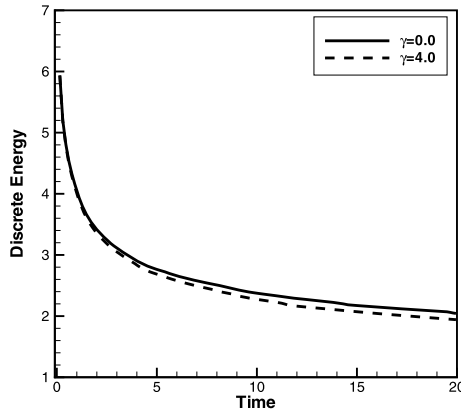


Fig. 4.3. Energy trace of numerical solution for Example 4.2.

should point out is that the energy is always non-increasing in time regardless of the parameter values of the space or time step sizes.

Example 4.3 (Buoyancy-driven flows). To simulate buoyancy-driven flow, we replace the Brinkman flow (2.1b) by

$$-\nabla \cdot [v(\phi)D(\mathbf{u})] + \eta(\phi)\mathbf{u} + \nabla p = -\gamma\phi\nabla\mu + \mathbf{b}, \tag{4.3}$$

where \mathbf{b} is a buoyancy term that depends on the mass density. The mass density is assumed depend on ϕ , i.e. $\rho = \rho(\phi)$, and we employ a Boussinesq type approximation:

$$\mathbf{b} = -b(\phi)\hat{\mathbf{k}}, \quad b(\phi) = \chi(\phi - \phi_0), \tag{4.4}$$

where ϕ_0 is a constant (usually the average value of ϕ), and χ is a constant. Thus, the corresponding convex-splitting scheme that we use for the buoyancy-driven flow is (3.1) with (3.1c) replaced by

$$-\nabla \cdot [v(\phi^n)D(\mathbf{u}^{n+1})] + \eta(\phi^n)\mathbf{u}^{n+1} = -\nabla p^{n+1} - \gamma\phi^n\nabla\mu^{n+1} - b(\phi^n)\hat{\mathbf{k}}. \tag{4.5}$$

The test involves the simulation of the buoyancy-driven flow with different values of γ . Again, we consider the convex splitting scheme with the LDG spatial discretization with \mathcal{P}^2 approximation on a 128×128 mesh and boundary conditions (2.5)–(2.6). The physical parameters are $\epsilon = 0.03$, $\phi_0 = \bar{\phi} = -0.05$, $\chi = 10$, $\eta = 1$ and $\nu = 1$. We take the mobility to be

$$M(\phi) = \sqrt{(1 + \phi)^4(1 - \phi)^4 + \epsilon^2}. \tag{4.6}$$

The initial data is a random field of values that are uniformly distributed about the average composition $\bar{\phi} = -0.05$, with amplitude 0.05. The domain is $[0, 6.4] \times [0, 6.4]$. For γ we use the values 2.0 and 4.0.

The simulation of the buoyancy-driven flow is shown in Fig. 4.4. As expected, the mixture phase separates into domains wherein $\phi \approx 1$ and $\phi \approx -1$. After a very rapid phase separation process, the blue phase ($\phi \approx -1$) sinks and the red phase ($\phi \approx 1$) rises. The fluids mix in complicated ways as this process occurs. The numerical results compare very well with the numerical calculations performed by Collins et al. [12].

Example 4.4 (Boundary-driven flows). We consider the last case, i.e. the boundary-driven flow. Specifically, we simulate the deformation of a particle in shear flow. We also consider the convex splitting scheme (3.1) with \mathcal{P}^2 approximation on a 128×128 mesh, and the boundary conditions are given as follows. Let $\mathbf{u} = (u, v)$ and $\Omega = [0, 6.4] \times [0, 6.4]$. We assume that all fields are periodic in the x direction, and we set at $y = 0$ and $y = 6.4$, $\partial_y\phi = \partial_y\mu = 0$, and $v = 0$. For the first component of the velocity vector, $u = \sigma$ at $y = 0$, and $u = -\sigma$ at $y = 6.4$, where $\sigma > 0$ is the shear rate.

The physical parameters are $M = 1$, $\epsilon = 0.03$, $\gamma = 4.0$, $\eta = 0$ and $\nu = 1$. The result of the boundary-driven simulation for $\sigma = 1$ and $\sigma = 2$ are reported in Fig. 4.5 and Fig. 4.6, respectively. From these figures, we can see that the shear rate is relatively modest, with respect to the surface tension, and the particle is stretched.

Finally, we remark that the numerical results presented above are qualitatively very similar to those presented in [12]. But, what we should have in mind is that the DG spatial discretization does allow for more flexibility than that of the finite difference method in several other ways. DG methods are a class of finite element methods, which can handle the irregular computational domain and complex boundary conditions easily comparing with the finite difference methods. Meanwhile, since the basis functions can be completely discontinuous, discontinuous Galerkin methods have the flexibility which is not shared by typical finite element methods, such as the allowance of arbitrary triangulation with hanging nodes, complete freedom in changing the polynomial degrees in each element independent of that in the neighbors (p -adaptivity), and

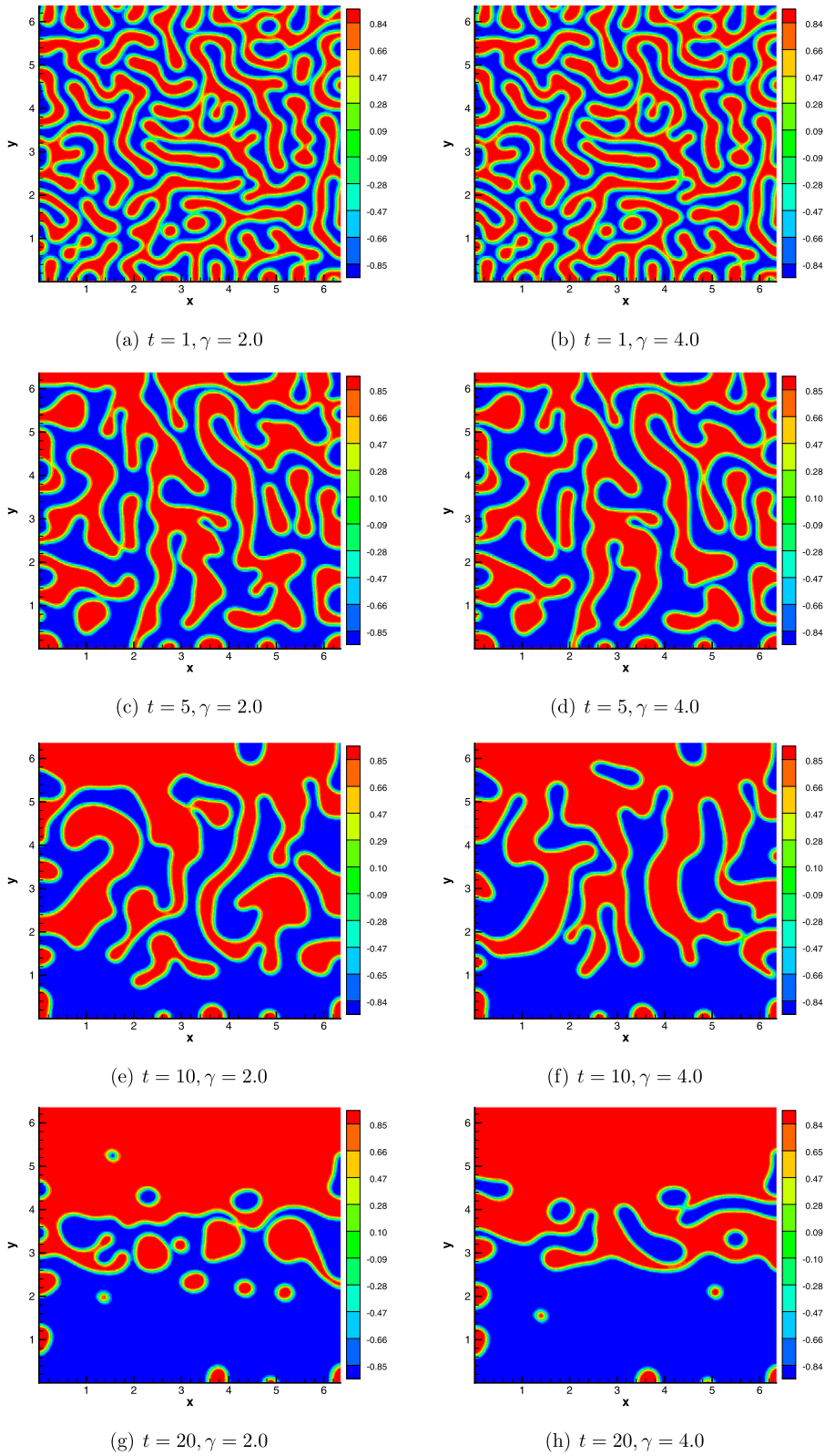


Fig. 4.4. The time evolution of the CHB system implemented with convex splitting scheme with \mathcal{P}^2 approximation on a 128×128 mesh for Example 4.3.

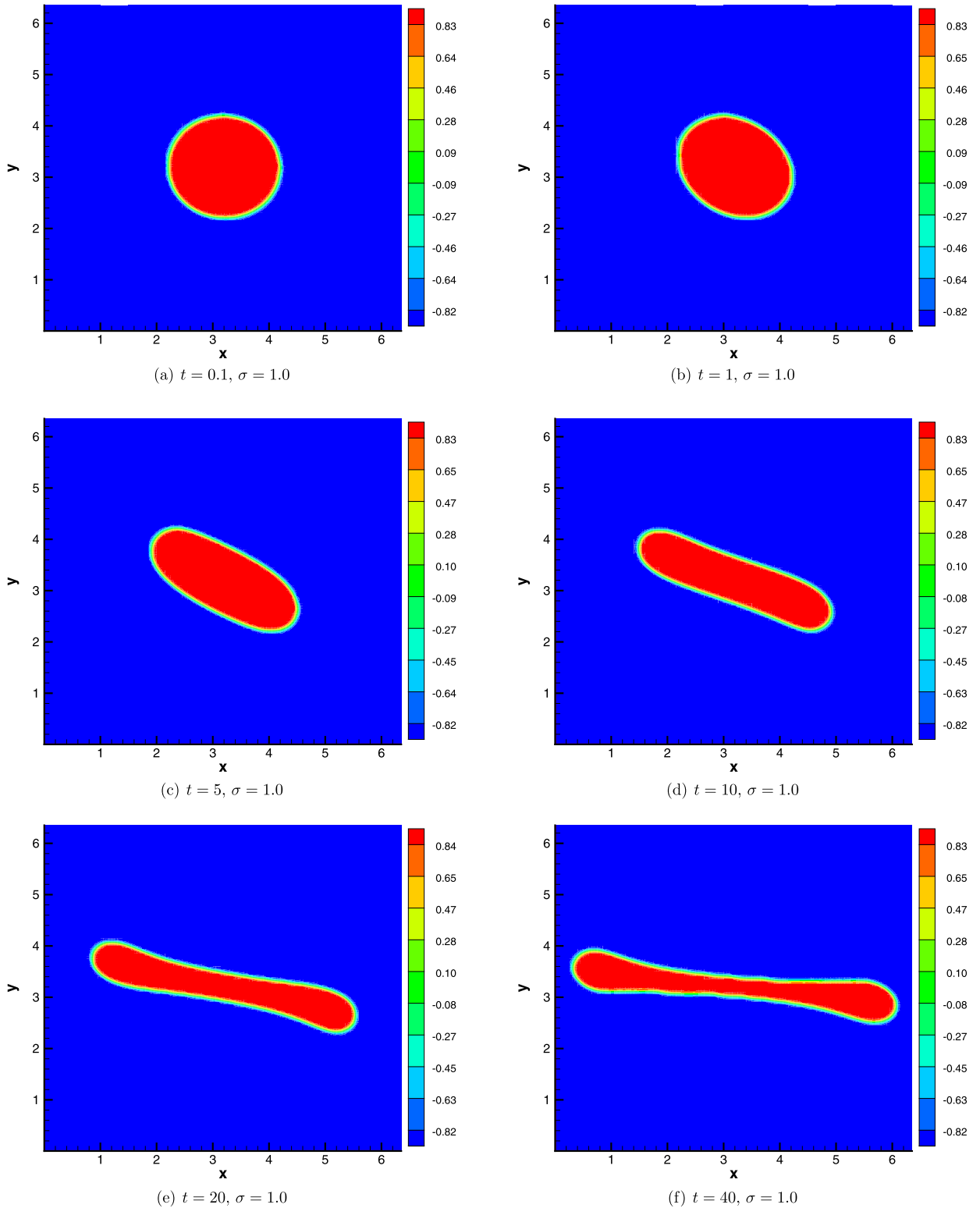


Fig. 4.5. The time evolution of the CHB system implemented with convex splitting scheme with \mathcal{P}^2 approximation on a 128×128 mesh for Example 4.4 with $\sigma = 1.0$.

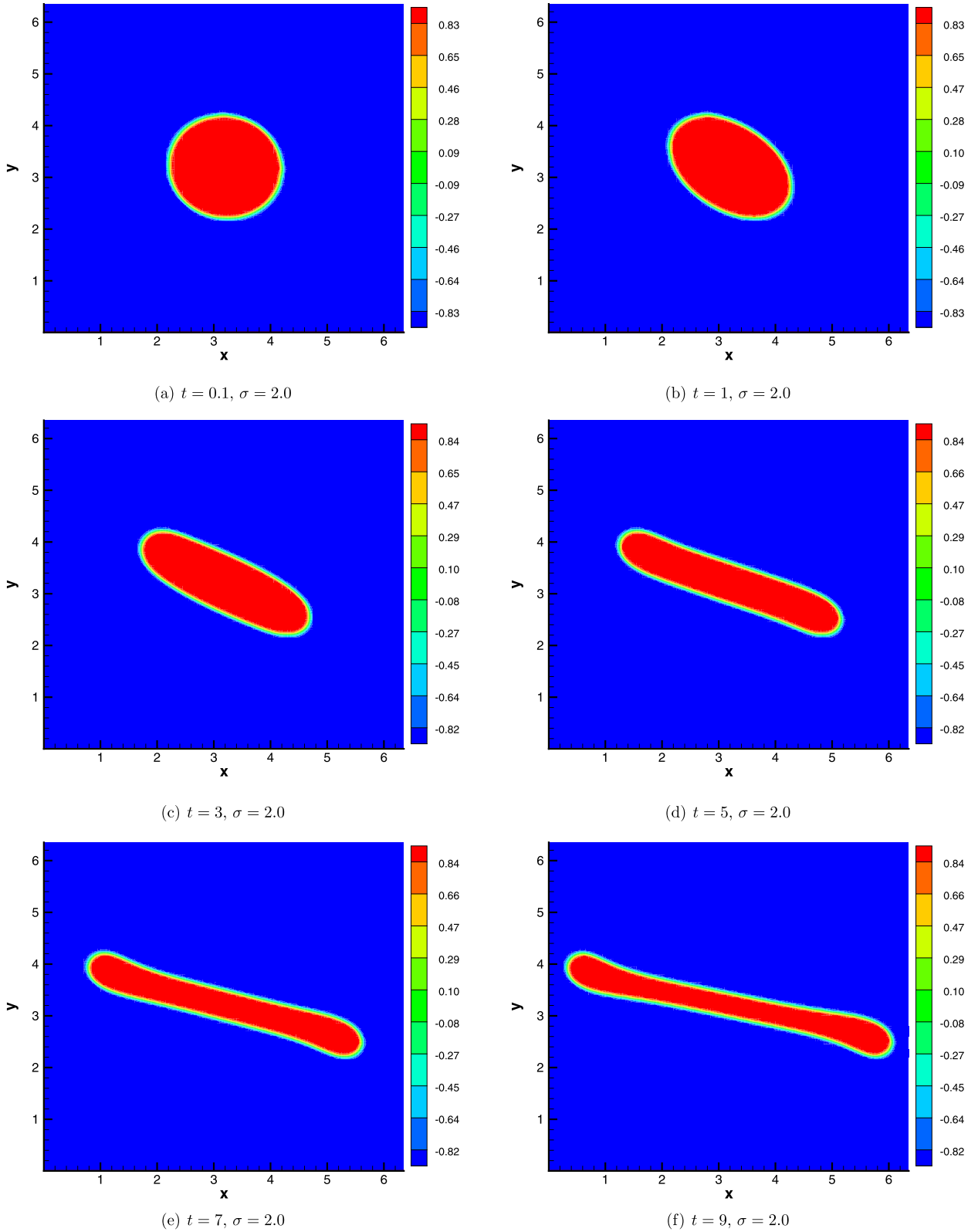


Fig. 4.6. The time evolution of the CHB system implemented with convex splitting scheme with \mathcal{P}^2 approximation on a 128×128 mesh for Example 4.4 with $\sigma = 2.0$.

extremely local data structure (elements only communicate with immediate neighbors regardless of the order of accuracy of the scheme) and the resulting embarrassingly high parallel efficiency.

5. Conclusion

In this paper, we have proposed a fully-discrete semi-implicit convex splitting method for approximating the Cahn–Hilliard–Brinkman system, which consists of the implicit Euler method combined with a convex splitting discrete Cahn–Hilliard energy strategy for the temporal discretization. The energy stability is proved for the semi-discrete scheme firstly. We also prove the unconditional energy stability for the fully-discrete semi-implicit LDG scheme. That is, the energy is always non-increasing in time regardless of time step sizes, which is observed in our computations and provides some evidence that our scheme is indeed stable. The semi-implicit method will result in a nonlinear system of algebraic equations at each time step and the FAS multigrid solver is employed to solve the system. We show numerically that the number of the multigrid iterations is nearly independent of the problem size and is of nearly optimal complexity. Numerical experiments based on the overall solution method of combining the fully-discrete convex splitting scheme and the nonlinear multigrid solver are presented to validate the theoretical results and to show the effectiveness of the proposed methods for approximating the Cahn–Hilliard–Brinkman phase field model. Although not addressed in this paper, the local discontinuous Galerkin method are flexible for general geometry, unstructured meshes and h and p adaptivity, and have excellent parallel efficiency.

References

- [1] J.W. Barrett, J.F. Blowey, Finite element approximation of a model for phase separation of a multi-component alloy with non-smooth free energy, *Numer. Math.* 77 (1997) 1–34.
- [2] J.W. Barrett, J.F. Blowey, H. Garcke, Finite element approximation of the Cahn–Hilliard equation with degenerate mobility, *SIAM J. Numer. Anal.* 37 (1999) 286–318.
- [3] J.W. Barrett, J.F. Blowey, H. Garcke, On fully practical finite element approximations of degenerate Cahn–Hilliard systems, *Math. Model. Numer. Anal.* 35 (2001) 713–748.
- [4] F. Bassi, S. Rebay, A high-order accurate discontinuous finite element method for the numerical solution of the compressible Navier–Stokes equations, *J. Comput. Phys.* 131 (1997) 267–279.
- [5] J.W. Cahn, On spinodal decomposition, *Acta Metall.* 9 (1961) 795–801.
- [6] B. Cockburn, C.-W. Shu, TVB Runge–Kutta local projection discontinuous Galerkin finite element method for conservation laws II: general framework, *Math. Comput.* 52 (1989) 411–435.
- [7] B. Cockburn, S.-Y. Lin, C.-W. Shu, TVB Runge–Kutta local projection discontinuous Galerkin finite element method for conservation laws III: one dimensional systems, *J. Comput. Phys.* 84 (1989) 90–113.
- [8] B. Cockburn, S. Hou, C.-W. Shu, The Runge–Kutta local projection discontinuous Galerkin finite element method for conservation laws IV: the multidimensional case, *Math. Comput.* 54 (1990) 545–581.
- [9] B. Cockburn, C.-W. Shu, The Runge–Kutta discontinuous Galerkin method for conservation laws V: multidimensional systems, *J. Comput. Phys.* 141 (1998) 199–224.
- [10] B. Cockburn, C.-W. Shu, The local discontinuous Galerkin method for time-dependent convection–diffusion systems, *SIAM J. Numer. Anal.* 35 (1998) 2440–2463.
- [11] B. Cockburn, G. Kanschat, D. Schötzau, C. Schwab, Local discontinuous Galerkin methods for the Stokes system, *SIAM J. Numer. Anal.* 40 (2002) 319–343.
- [12] C. Collins, J. Shen, S.M. Wise, An efficient, energy stable scheme for the Cahn–Hilliard–Brinkman system, *Commun. Comput. Phys.* 13 (2013) 929–957.
- [13] A.E. Diegel, X.H. Feng, S.M. Wise, Analysis of a mixed finite element method for a Cahn–Hilliard–Darcy–Stokes system, *SIAM J. Numer. Anal.* 53 (2015) 127–152.
- [14] D.J. Eyre, Systems of Cahn–Hilliard equations, *SIAM J. Appl. Math.* 53 (1993) 1686–1712.
- [15] X.B. Feng, S.M. Wise, Analysis of a Darcy–Cahn–Hilliard diffuse interface model for the Hele–Shaw flow and its fully discrete finite element approximation, *SIAM J. Numer. Anal.* 50 (2012) 1320–1343.
- [16] D. Furihata, A stable and conservative finite difference scheme for the Cahn–Hilliard equation, *Numer. Math.* 87 (2001) 675–699.
- [17] R. Guo, Y. Xu, Efficient solvers of discontinuous Galerkin discretization for the Cahn–Hilliard equations, *J. Sci. Comput.* 58 (2014) 380–408.
- [18] R. Guo, Y. Xia, Y. Xu, An efficient fully-discrete local discontinuous Galerkin method for the Cahn–Hilliard–Hele–Shaw system, *J. Comput. Phys.* 264 (2014) 23–40.
- [19] D. Kay, R. Welford, A multigrid finite element solver for the Cahn–Hilliard equation, *J. Comput. Phys.* 212 (2006) 288–304.
- [20] J. Kim, K. Kang, J. Lowengrub, Conservative multigrid methods for Cahn–Hilliard fluids, *J. Comput. Phys.* 193 (2004) 511–543.
- [21] J. Kim, K. Kang, J. Lowengrub, Conservative multigrid methods for ternary Cahn–Hilliard systems, *Commun. Math. Sci.* 2 (2004) 53–77.
- [22] H.G. Lee, J.S. Lowengrub, J. Goodman, Modeling pinchoff and reconnection in a Hele–Shaw cell. I. The models and their calibration, *Phys. Fluids* 14 (2002) 492–513.
- [23] H.G. Lee, J.S. Lowengrub, J. Goodman, Modeling pinchoff and reconnection in a Hele–Shaw cell. II. Analysis and simulation in the nonlinear regime, *Phys. Fluids* 14 (2002) 514–545.
- [24] W. Ngamsaad, J. Yojina, W. Triampo, Theoretical studies of phase-separation kinetics in a Brinkman porous medium, *J. Phys. A, Math. Theor.* 43 (2010) 202001.
- [25] W.H. Reed, T.R. Hill, Triangular mesh method for the neutron transport equation, Technical report LA-UR-73-479, Los Alamos Scientific Laboratory, Los Alamos, NM, 1973.
- [26] Z.Z. Sun, A second-order accurate linearized difference scheme for the two-dimensional Cahn–Hilliard equation, *Math. Comput.* 64 (1995) 1463–1471.
- [27] U. Trottenberg, C. Oosterlee, A. Schüller, *Multigrid*, Academic Press, New York, 2005.
- [28] S.M. Wise, Unconditionally stable finite difference, nonlinear multigrid simulation of the Cahn–Hilliard–Hele–Shaw system of equations, *J. Sci. Comput.* 44 (2010) 38–68.
- [29] Y. Xia, Y. Xu, C.-W. Shu, Local discontinuous Galerkin methods for the Cahn–Hilliard type equations, *J. Comput. Phys.* 227 (2007) 472–491.
- [30] Y. Xia, Y. Xu, C.-W. Shu, Application of the local discontinuous Galerkin method for the Allen–Cahn/Cahn–Hilliard system, *Commun. Comput. Phys.* 5 (2009) 821–835.

- [31] Y. Xu, C.-W. Shu, Local discontinuous Galerkin methods for high-order time-dependent partial differential equations, *Commun. Comput. Phys.* 7 (2010) 1–46.
- [32] J. Yan, C.-W. Shu, A local discontinuous Galerkin method for KdV type equations, *SIAM J. Numer. Anal.* 40 (2002) 769–791.
- [33] J. Yan, C.-W. Shu, Local discontinuous Galerkin methods for partial differential equations with higher order derivatives, *J. Sci. Comput.* 17 (2002) 27–47.